

IEEE Access

Multidisciplinary | Rapid Review | Open Access Journal



Search IEEE Access

- About IEEE Access
- Rapid Peer Review
- Benefits of Publishing
- Topical Sections
- Guide for Authors
- Editorial Leadership



IEEE Access is a multidisciplinary, open access journal of the IEEE.

Continuously presenting the results of original research or development across all of IEEE's fields of interest, IEEE Access provides authors a high-quality open access journal with a rapid yet rigorous peer review process of 4 to 6 weeks.

[Learn More](#)

Share this page



System

Read more

Optimization

Read more

Coplanar Waveguide Terminated With an Open Complementary Split Ring Resonator (OCSRR)

Read more

More Featured Articles

- Improving Predictability of User-Affecting Metrics to Support Anomaly Detection in Cloud Services
- Robots Under COVID-19 Pandemic: A Comprehensive Survey
- Artificial Intelligence and COVID-19: Deep Learning Approaches for Diagnosis and Treatment
- Phantom Malware: Conceal Malicious Actions From Malware Detection Techniques by Imitating User Activity
- Absorption of 5G Radiation in Brain Tissue as a Function of Frequency, Power and Time

Announcements

Enter for a chance to win a \$500 USD Amazon gift card!

- Enter the Best Video Award for the Opportunity to Win \$500
- Five IEEE Access Editorial Board Members Recognized as Highly Cited Researchers by Web of Science™
- Winners of the 2019 IEEE Access Best Multimedia Award (Part 2)
- How to Get Published in IEEE Access, by Editor-in-Chief, Derek Abbott

FAQ

Read answers to common questions:

- What is the scope?
- What is the criterion for acceptance?
- Who reads IEEE Access?
- What kind of authors publish?
- Is it indexed?
- Does it have an impact factor?

[View FAQ](#)

Home » Editorial Leadership » Editorial Board

Editorial Board

[+ Find alphabetically](#)

Share this page:



Ram Adapa
Electric Power Research Institute, Palo Alto, California, USA



Anuradha Annaswamy
MIT, Cambridge, Massachusetts, USA



Nirwan Ansari
New Jersey Institute of Technology, Newark, New Jersey, USA



Jun Cai
Concordia University, Canada, Montreal, Quebec, Canada



José Capmany
Universitat Politècnica de València, València, Spain



Kun-Shan Chen
Guilin University of Technology, Guangxi, China



J.-C. Chiao
Southern Methodist University, Dallas, TX, USA



M. Jamal Deen
McMaster University, Hamilton, Ontario, Canada



John W. Evans
NASA, Washington, DC, USA



Shaikh Anowarul Fattah
Bangladesh University of Engineering and Technology (BUET), Dhaka, Bangladesh



Aura Ganz
University of Massachusetts, Amherst, Massachusetts, USA



Amitava Ghosh
Nokia Networks, Buffalo Grove, Illinois, USA



Dmitry Goldgof
University of South Florida, Tampa, Florida, USA



Josep M. Guerrero
Aalborg University, Aalborg, Denmark



Melinda Hodkiewicz
University of Western Australia, Perth, Australia



Abbas Jamalipour
University of Sydney, Sydney, Australia



Weihua Jiang
Nagaoka University of Technology, Nagaoka, Niigata, Japan



Lina Karam
Lebanese American University, Beirut, Lebanon



Okyay Kaynak
Bogaziçi University, Istanbul, Turkey



Joy Laskar
Maja Systems, Milpitas, California, USA



Gianluca Lazzi
University of Southern California, Los Angeles, California, USA



Victor Leung
The University of British Columbia, Vancouver, British Columbia, Canada



Shengtao Li
Xi'an Jiaotong University, China



Qilian Liang
University of Texas at Arlington, Arlington, Texas, USA



Jian-Yu Lu
The University of Toledo, Toledo, Ohio, USA



Leda Lunardi
North Carolina State University, Raleigh, NC, USA



Michael G Pecht
University of Maryland, College Park, Maryland, USA



Mugen Peng
Beijing University of Posts and Telecommunications, Beijing, China



Hugo Proença
University of Beira Interior, Covilhã, Portugal



Yi Qian
University of Nebraska-Lincoln, Lincoln, Nebraska, USA



Zihua Qu
University of Central Florida,
Orlando, Florida, USA



Mehrdad Saif
University of Windsor,
Windsor, Ontario, Canada



Ali Serpengüzel
Koç University,
Istanbul, Turkey



Levent Sevgi
Okan University,
Istanbul, Turkey



Ashitey Trebi-Ollennu
NASA-JPL California Institute
of Technology,
Pasadena, California, USA



Leung Tsang
The University of Michigan,
Ann Arbor, Michigan, USA




































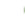


Ge Wang
Rensselaer Polytechnic Institute,
Troy, New York, USA



Andreas Weisshaar
Oregon State University,
Corvallis, Oregon, USA



Enrico Zio
Mines ParisTech (France), Politecnico di
Milano (Italy),
Paris, France, Milano, Italy

-
- Deep Reinforcement Learning-Based Tie-Line Power Adjustment Method for Power System Operation State Calculation** 
Huating Xu; Zhihong Yu; Qingping Zheng; Jinxiu Hou; Yawei Wei; Zhijian Zhang
Publication Year: 2019 , Page(s): 156160 - 156174
Cited by: Papers (1)
[▶ Abstract](#) [\(html\)](#)  (8239 Kb) 
-
- Real-Time Quadruple-Frequency Cycle Slip Detection and Repair Algorithm Based on the Four Chosen Linear Combinations** 
Yaoding Wang; Ke Zhang; Wenxiang Liu; Zhengrong Li; Feixue Wang
Publication Year: 2019 , Page(s): 154697 - 154710
[▶ Abstract](#) [\(html\)](#)  (5488 Kb) 
-
- Multi-MC Charging Schedule Algorithm With Time Windows in Wireless Rechargeable Sensor Networks** 
Zhenchun Wei; Meng Li; Qing Zhao; Zengwei Lyu; Siwei Zhu; Zhen Wei
Publication Year: 2019 , Page(s): 156217 - 156227
[▶ Abstract](#) [\(html\)](#)  (5434 Kb) 
-
- Multi-Objective Machining Parameters Optimization for Chatter-Free Milling Process Considering Material Removal Rate and Surface Location Error** 
Congying Deng; Yi Feng; Jianguo Miao; Ying Ma; Bo Wei
Publication Year: 2019 , Page(s): 183823 - 183837
[▶ Abstract](#) [\(html\)](#)  (2950 Kb) 
-
- Intelligent Quality of Service Routing in Software-Defined Satellite Networking** 
Shuai Wu; Lei Yang; Jianming Guo; Quan Chen; Xianfeng Liu; Chengguang Fan
Publication Year: 2019 , Page(s): 155281 - 155298
[▶ Abstract](#) [\(html\)](#)  (4385 Kb) 
-
- Social Network-Oriented Learning Agent for Improving Group Intelligence Coordination** 
Jingtiao Qi; Liang Bai; Yandong Xiao
Publication Year: 2019 , Page(s): 156526 - 156535
Cited by: Papers (1)
[▶ Abstract](#) [\(html\)](#)  (3338 Kb)  [Media](#)
-
- Automatic Detection of Single Ripe Tomato on Plant Combining Faster R-CNN and Intuitionistic Fuzzy Set** 
Chunhua Hu; Xuan Liu; Zhou Pan; Pingping Li
Publication Year: 2019 , Page(s): 154683 - 154696
Cited by: Papers (5)
[▶ Abstract](#) [\(html\)](#)  (1452 Kb) 
-
- H_∞ Consensus of Linear Multi-Agent Systems With Semi-Markov Switching Network Topologies and Measurement Noises** 
Meiyan Cong; Xiaowu Mu
Publication Year: 2019 , Page(s): 156089 - 156096
Cited by: Papers (2)
[▶ Abstract](#) [\(html\)](#)  (7185 Kb) 
-
- Directional Modulation Design Under a Constant Magnitude Constraint for Weight Coefficients** 
Bo Zhang; Wei Liu; Yang Li; Xiaonan Zhao; Cheng Wang
Publication Year: 2019 , Page(s): 154711 - 154718
Cited by: Papers (4)
[▶ Abstract](#) [\(html\)](#)  (6185 Kb) 
-
- Mission Planning and Control of Multi-Aircraft Systems With Signal Temporal Logic Specifications** 
Bariş Başpınar; Hamsa Balakrishnan; Emre Koyuncu
Publication Year: 2019 , Page(s): 155941 - 155950
Cited by: Papers (1)
[▶ Abstract](#) [\(html\)](#)  (3320 Kb) 
-
- Distributed Clustering of Text Collections** 
Juan Zamora; Héctor Allende-Cid; Marcelo Mendoza
Publication Year: 2019 , Page(s): 155671 - 155685
[▶ Abstract](#) [\(html\)](#)  (7953 Kb) 
-
- Enhanced NO Gas Performance of (002)-Oriented Zinc Oxide Nanostructure Thin Films** 
Fitriana; Ni Luh Wulan Septiani; Damar Rastri Adhika; Adhitya Gandaryus Saputro; Nugraha; Brian Yulianto
Publication Year: 2019 , Page(s): 155446 - 155454
Cited by: Papers (2)
[▶ Abstract](#) [\(html\)](#)  (8937 Kb) 

Received August 15, 2019, accepted October 17, 2019, date of publication October 24, 2019, date of current version November 6, 2019.

Digital Object Identifier 10.1109/ACCESS.2019.2949463

Enhanced NO Gas Performance of (002)-Oriented Zinc Oxide Nanostructure Thin Films

FITRIANA¹, NI LUH WULAN SEPTIANI¹, DAMAR RASTRI ADHIKA^{1,2},
ADHITYA GANDARYUS SAPUTRO^{1,2}, NUGRAHA^{1,2},
AND BRIAN YULIARTO^{1,2}

¹Advanced Functional Materials Research Group, Institut Teknologi Bandung, Bandung 40132, Indonesia

²Research Center for Nanosciences and Nanotechnology, Institut Teknologi Bandung, Bandung 40132, Indonesia

Corresponding author: Brian Yulianto (brian@tf.itb.ac.id)

This work was partially funded by Indonesia Endowment Fund for Education (LPDP), Ministry of Finance of Republic of Indonesia, Institut Teknologi Bandung (ITB), and Indonesian Ministry of Research and higher Education under World Class University (WCU) Program managed by Institut Teknologi Bandung.

ABSTRACT (002)-oriented ZnO nanostructure for NO gas sensing application was successfully grown on glass substrates by two-step processes, which are seeding process via dip-coating method using diethanolamine (DEA) as chelating agent and growth process via chemical bath deposition (CBD). The samples were characterized by X-ray diffraction (XRD), scanning electron microscopy (SEM), and transmission electron microscopy (TEM). Two ZnO film samples, named samples A and B, were fabricated without and with DEA addition in the seeding process, respectively. XRD observation results show that ZnO film was successfully deposited on both samples, where sample A has a random crystal orientation; while sample B has a very dominant (002) orientation. Further, the selected area electron diffraction (SAED) observation with TEM confirmed that sample A has a random orientation indicated by a ring-shaped diffraction pattern; while sample B has a hexagonal crystalline structure diffraction pattern which is oriented towards the normal direction of the substrate surface, indicated that ZnO film was grown along this (002) orientation for sample B. SEM images of both samples showed that the ZnO film is ZnO nanorods with hexagonal wurtzite structure shape and sample A is clearly more randomly oriented than sample B. During the investigation of NO gas sensing performance, it is found that the highest response towards NO gas was occurred at a lower operating temperature of 200°C for sample B compared to a higher operating temperature of 300°C for sample A. Furthermore, sample B has a higher dynamic gas response and sensitivity than sample A. These results indicate that the (002) oriented ZnO film has a better performance than the randomly oriented ZnO film as NO gas sensor.

INDEX TERMS Gas sensor, nitric oxide, orientation, ZnO.

I. INTRODUCTION

Recently, the rapid development of industrial technology encourages the increase of air pollution due to the production of exhaust gases such as a nitric oxide (NO), by industrial activities. These gases can cause irritation of the eyes and respiratory system even though in low concentration, while in higher concentration, it can cause death [1]. Unfortunately, these gases cannot be detected by human senses because they are colorless and odorless. To solve this problem, different kinds of materials have been developed as a gas sensor [2].

The associate editor coordinating the review of this manuscript and approving it for publication was Rahul A. Trivedi.

ZnO is an II-IV semiconductor material that has a wide direct bandgap (3.37 eV), large exciton binding energy (60 meV), high electron mobility, non-toxicity, tunable morphology, good chemical and thermal stability. These characteristics make ZnO being one of the promising material which is widely used as gas sensor [3]–[5]. Many factors can affect the performance of ZnO as a gas sensor, one of them is ZnO crystalline orientation [6]–[8]. ZnO thin film with (002) growth orientation, where the c-axis of ZnO growth perpendicular to the substrate, is widely utilized for many different purposes such as field effect transistor [9], gas sensor [10], [11], surface acoustic wave (SAW) [12], photocatalysis [13], photovoltaic [14] and piezoelectric devices [15].

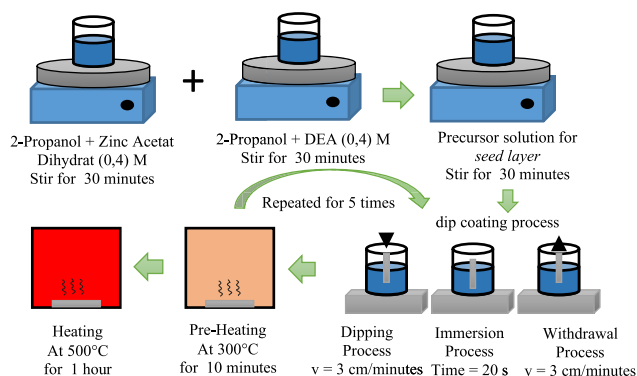


FIGURE 1. Experimental procedure of ZnO seed layer formation.

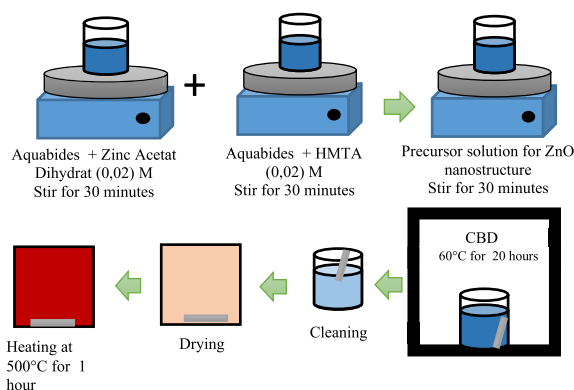


FIGURE 2. Experimental procedure of ZnO nanostructure formation.

The (002)-oriented ZnO films can be prepared using various methods including sol gel method [16], [17], chemical bath deposition (CBD) [18], [19], magnetron sputtering [20], plasma-enhanced chemical vapor deposition (PECVD) [21], and pulsed layer deposition (PLD) [22]. Among them, CBD method is selected in this experiment due to its simple, low cost, easy, and large area deposition result [23], [24]. Diethanolamine (DEA) is a chelating agent that mostly used in the sol-gel method to prepare ZnO. However, reports on ZnO growth tendency along (002) orientation using DEA as a chelating agent are still rarely found in the literature [25]. In this study, (002)-oriented ZnO thin film on a glass substrate has been successfully fabricated using DEA. The gas sensing properties of (002) oriented ZnO nanorod and randomly ZnO nanorod are compared in order to find the effect of the growth orientation to the NO gas sensor properties.

II. EXPERIMENTAL

The ZnO films were prepared by two-step process namely seeding process using dip-coating method as is shown in Fig.1 and growth process using chemical bath deposition (CBD) as is shown in Fig.2. The substrate used in this work was silica glass that was cleaned by ethanol and deionized water using ultrasonic bath in sequence prior to the process.

A. SEEDING PROCESS

ZnO seed layers were synthesized via dip-coating method using zinc acetate dihydrate ($\text{Zn}(\text{CH}_3\text{COO})_2 \cdot 2\text{H}_2\text{O}$) as a zinc source. The preparation of precursor solution for ZnO seed layer was described as follows; 0.4 M $\text{Zn}(\text{CH}_3\text{COO})_2 \cdot 2\text{H}_2\text{O}$ and 0.4 M DEA ($\text{HN}(\text{CH}_2\text{CH}_2\text{OH})_2$) were first dissolved separately in 2-propanol solution at room temperature for 30 minutes. Subsequently, both solutions were mixed for 30 minutes using a magnetic stirrer. A multilayer (5 layers) of ZnO seed was deposited onto the glass substrates by dipping the glass substrates into the prepared solution and withdrawing it at the speed of 3.0 cm/min followed by drying process at 300°C for 10 min of each layer. Finally, the prepared multilayer films were post-heated at 500°C for 1 hour. The same procedure but without DEA was also performed to investigate its effect on the growth orientation. Two ZnO film samples named samples A and B, were fabricated without and with DEA addition in the seeding process, respectively.

B. GROWTH PROCESS

During growth process of ZnO nanostructure, precursor solution was prepared by dissolving zinc acetate dihydrate and HMTA separately and then mixed those solutions together using a magnetic stirrer for 30 minutes. The concentration of zinc acetate dihydrate and HMTA were 0,02 M with equimolar ratio. After stirring process, the resultant solution was transferred into a beaker glass where the seeded glass substrate were placed vertically inside the glass. The solution temperature was maintained at 60°C for 20 hours. After cooling process, the glass substrate was rinsed with deionized water followed by drying at 100°C for 15 minutes and post-heating at 500°C for 1 hour.

C. CHARACTERIZATION

Both ZnO film samples, A and B, were characterized in order to elucidate their structure, orientation, and morphology. XRD spectra were examined using Bruker D8 Advance Diffractometer with a $\text{Cu-K}\alpha$ radiation ($\lambda = 1.54 \text{ \AA}$) and operating voltage of 40 kV and current of 40 mA. XRD observation were carried out with 2θ range of 20°-70°, step length of 0.02° and scan rate of 5°/min. The morphology of ZnO film samples was observed by SEM Hitachi SU3500 operating at an accelerating voltage of 10 kV. The orientation of ZnO film samples were elucidated using SAED method in HRTEM Hitachi H9500 with an accelerating voltage of 300 kV. TEM samples were fabricated using micro-sampling method on focused ion beam (FIB) Hitachi FB2200 with 40-20 kV operating voltage.

D. GAS RESPONSE TESTING OF ZNO FILM

Investigation on gas sensing characteristic of both ZnO film samples, A and B, were conducted in a gas sensing system. The gas responses were obtained by measuring the resistance of ZnO film under various operating temperature (160°C, 200°C, 250°C, 300°C, and 350°C) and NO gas concentration

(10 ppm, 30 ppm, 50 ppm, 70 ppm, and 90 ppm). Then the dynamic gas response is defined as [26]:

$$\text{Response} = \left(\frac{R_a - R_g}{R_a} \right) \times 100\% \quad (1)$$

where R_a and R_g are resistance of the ZnO film in dry air and gas target (NO) atmosphere, respectively. In this measurement, the NO gas was mixed with Nitrogen as a carrier gas to control the concentration of NO. Since nitrogen is an inert gas, there is no reaction occurred between the nitrogen and NO gas. Before exposed to NO, dry air was introduced to the samples in the testing chamber until a stable state of resistance was obtained. Subsequently, the samples were exposed to NO gas at a certain concentration for 10 min followed by cleaning phase using dry air to reach a stable resistance.

E. DFT CALCULATION

We simulate the adsorption NO gas on ZnO(100) surface using density functional theory-based (DFT) calculations [27], [28]. Spin-polarized DFT calculations is performed using the Quantum-Espresso 5.4 [29]. Exchange and correlation effects are incorporated within the generalized gradient approximation, using the Perdew-Burke-Ernzerhof (PBE) functional [27]. We use plane wave basis sets with 42 Ry cut-off energy. Valence-core interactions are represented by the projector augmented wave formalism (PAW) [30]. The Brillouin zone sampling for all systems, except isolated molecule, are performed with a $2 \times 2 \times 1$ k-point mesh for the structural and electronic properties. Calculation for isolated molecule is done at the gamma point in a $30 \times 30 \times 30 \text{ \AA}$ cubic cell. Hubbard-U correction is added by amount of 7.5 eV for Zn 3d states, following refs. [31], [32]. The effect of van der Waals interaction is described using the semi-empirical correction scheme of Grimme (DFT-D2) [33]. The systems are relaxed until the residual force on each atomic component is less than 0.025 eV/\AA .

The non-polar ZnO (100) surface is modeled by repeated slab approach where the slabs are separated by vacuum space of about 15 \AA . The slab model contains eight layers of Zn-O using a 2×2 supercell. The surface model is shown in Fig. 3. In all of the adsorption cases, atoms in adsorbed molecules and in two topmost Zn-O layer are fully relaxed during optimization, while the rest are fixed in their bulk positions. Visualization of atomic structures and charge density are done by using Xcrysden software [34]. Saddle points of some reactions are calculated by the nudged elastic band method (NEB) [35]–[37].

III. RESULTS AND DISCUSSION

A. STRUCTURE, ORIENTATION, AND MORPHOLOGY OF ZNO FILM

XRD measurement was performed on both ZnO film samples, A and B, to find out the structural information of the prepared ZnO films. The XRD patterns are shown in Fig.4 where Fig.4(a) shows the XRD pattern of sample A and Fig.4(b)

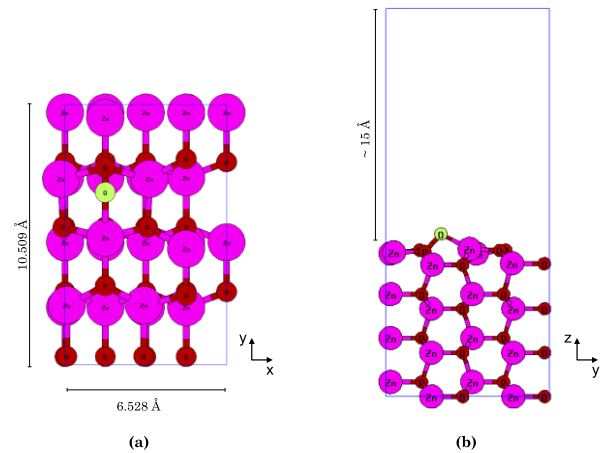


FIGURE 3. The top view (a) and side view (b) of unit cell model of ZnO(100) surface with an adsorbed O atom (O^{ads} site).

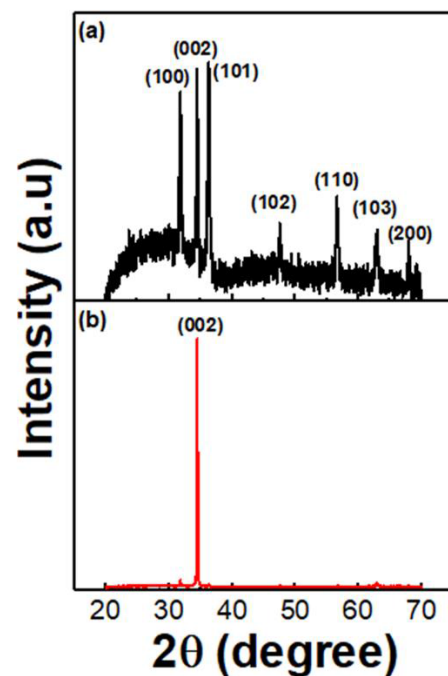


FIGURE 4. XRD pattern of ZnO films synthesized (a) without DEA (sample A) (b) using DEA (sample B).

shows the XRD pattern of sample B. All of the diffraction peaks consistent with the wurtzite hexagonal zinc oxide phase based on JCPDS (Joint Committee on Powder Diffraction Standards) card number 36-1451.

XRD pattern of the sample A which was synthesized without DEA in Fig.4(a), shows several peaks at 2θ of 31.8° , 34.4° , and 36.2° . Those peaks are assigned to (100), (002), and (101) planes, respectively. That pattern confirms that ZnO nanorods in sample A were grown with random orientation. Whereas, XRD pattern of sample B which was synthesized using DEA in Fig.4(b), shows one dominant peak at $2\theta = 34.4^\circ$ which is assigned to (002) ZnO plane. That peak

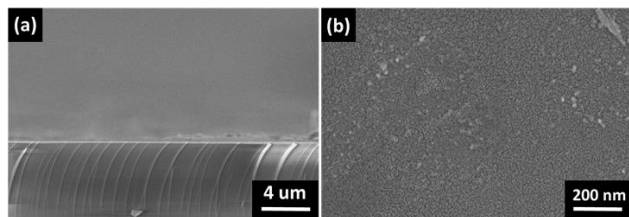


FIGURE 5. Cross section (a) and top view (b) of SEM images of ZnO seed synthesized by dip coating method.

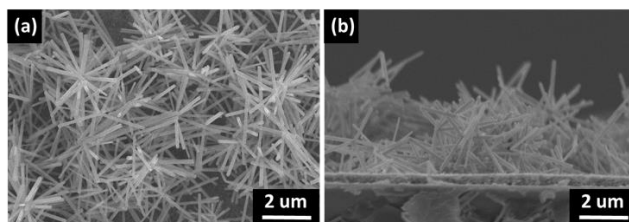


FIGURE 6. SEM images of ZnO films synthesized without DEA (sample A) (a) top view (b) cross section view.

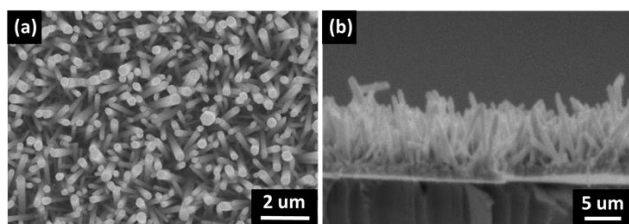
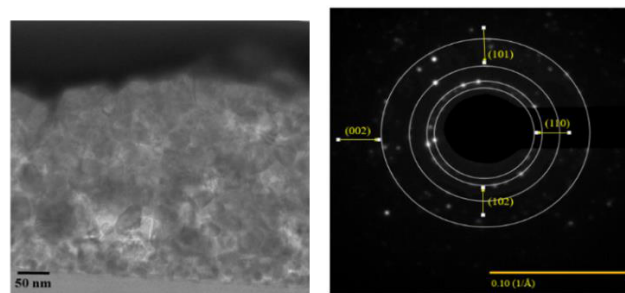


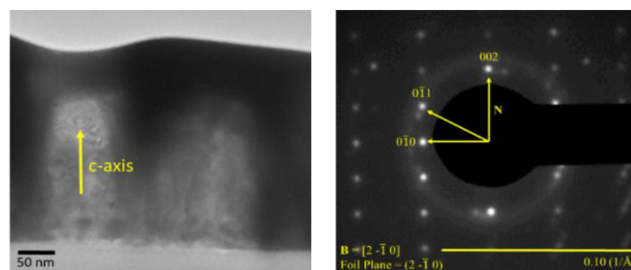
FIGURE 7. SEM images of ZnO films synthesized using DEA (sample B) (a) top view (b) cross section view.

suggested that the ZnO film growth along (002) orientation. Furthermore, the peak has a sharp and strong intensity, indicated that sample B has a good crystallinity. Based on this result, we can conclude that the presence of DEA in the seed layer precursor solution can affect the orientation of ZnO. That phenomenon can be explained as follows; The role of DEA as complexing agent allow the formation of zinc oxyacetate and condensation of Zn^{2+} . The amine group in the DEA can increases the condensation rate of Zn^{2+} ions along the ZnO plane which has minimum surface energy ((002) plane). This condition encourages the growth of ZnO along c-axis resulting preferable (002)-oriented ZnO [38].

The morphology of ZnO films were characterized using SEM as are shown in Fig.5, 6 and 7. The seed layer was successfully deposited on the substrate with thickness ~ 600 nm and no rod was observed on the substrate (Fig. 5 (a,b)). It could be seen from Fig. 6(a) and 7(a) that both samples A and B have the same structure, nanorods with hexagonal shape with the diameter of about 80 nm. Cross-section SEM images in Fig. 6(b) and 7(b) show that ZnO nanorods of sample A were grown randomly, while most of ZnO nanorods of sample B were grown towards one certain direction. Furthermore, the length of ZnO nanorods of sample A is $1.6 \mu m$, which is twice the length of nanorod of sample B.



(a)



(b)

FIGURE 8. TEM images (left) and SAED patterns (right) of ZnO films synthesized (a) without DEA in (sample A) (b) with DEA (sample B) in seeding process.

The difference of the length is due to the oriented nanorod need more energy to grow than the random nanorod. Moreover, from cross section SEM image, the length of oriented nanorods indicated the thickness of the thin film, which is less than $1 \mu m$ and belong to thin film category, while the average thickness of random nanorods is more than $1 \mu m$ and belong to thick film category.

TEM images and their SAED patterns of ZnO film, A and B, can be seen in Fig.8(a) and 8(b), respectively. The TEM images in Fig.8(a) and 8(b) shows three layers with different contrast where the bright base layer indicates glass substrate, the center layer shows ZnO nanorods, and the dark top layer shows tungsten layer that was deposited during FIB fabrication for sample protection during ion beam thinning process. SAED pattern in Fig.8(a) shows several circular patterns indicating that ZnO nanorods are oriented randomly on sample A. The radius of the circles in the SAED pattern in Fig.8(a) indicate the d_{hkl} values for (110), (101), (110), and (002) ZnO planes, which is in a good agreement with the result obtained from XRD spectrum for sample A. Moreover, SAED pattern in Fig.8(b) shows hcp crystal zone axis pattern for (2-10) foil plane. The g-vector analysis on the observed diffraction spots show the normal direction of each plane, that are (002), (0-11), and (0-10) as shown by yellow arrows in Fig.8(b). It is known that the normal direction of (002) plane, that is parallel to the direction of ZnO nanorod c-axis, is oriented towards normal direction of glass substrate, confirming the XRD spectrum result for sample B, that the ZnO nanorods were grown along (002) orientation in sample B.

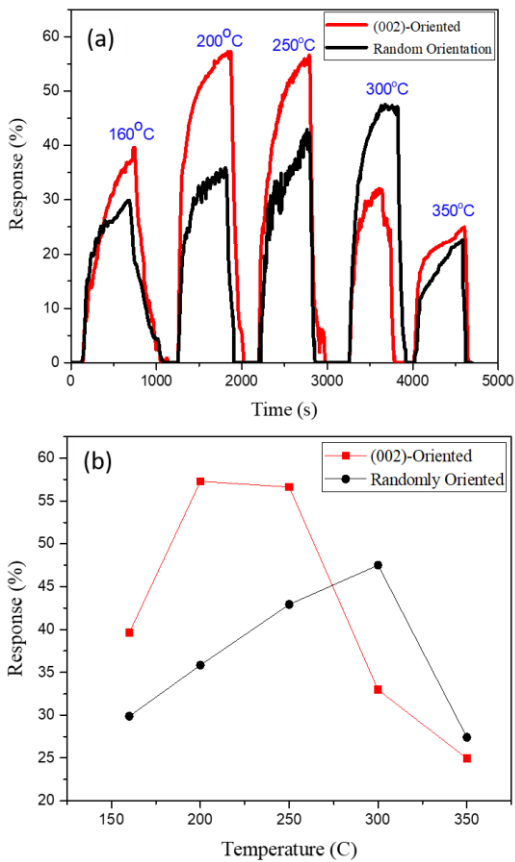


FIGURE 9. The dynamic response characteristic of ZnO films (a) and ZnO films response value to 30 ppm NO (b) at various temperature.

B. GAS SENSING PROPERTIES

In this work, we compare the gas sensing properties between sample A and B to find out the effect of the growth orientation on NO gas sensing properties. ZnO film dynamic gas responses was measured according to the method described in experimental section. In this case, the DEA is indirectly affecting the NO gas measurement result. The used of DEA in seeding process result in (002) oriented nanorod which has more active site for gas exposure than random nanorod will give better sensing activities. Fig.9 shows the response of ZnO films to 30 ppm NO gas at different temperatures to investigate the optimum working temperature of ZnO films. The optimum working temperature is defined as the temperature where ZnO nanorods films show the highest response [39]. It can be seen that the response of ZnO films changes when the temperature was varied between 160°C-350°C. Firstly, the response was increasing up to 47.5% as the temperature increase to 300°C for sample A and up to 57.28% as temperature increase to 200°C for sample B, then the response keep decreasing at higher temperatures. The response has a tendency to increase and reach the maximum at an optimum temperature and then decreasing with temperature increase. This tendency was observed commonly in many previous studies [40]–[44]. It might be caused by

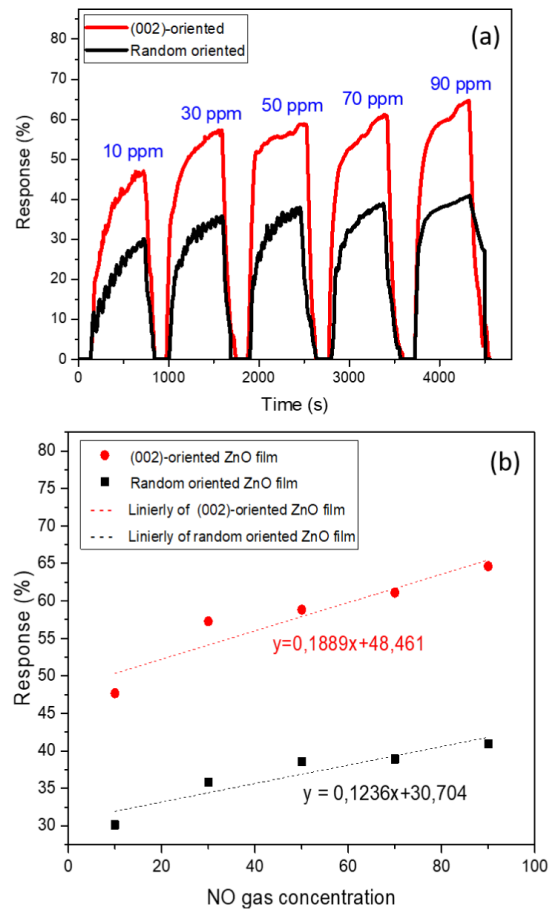


FIGURE 10. (a) The dynamic gas response characteristic of ZnO films at various NO gas concentration (b) ZnO films response to NO gas with different concentration.

low kinetics at temperatures lower than the optimum working temperature and by the increasing of desorption rate at temperatures higher than optimum working temperature [45]. According to this result, we can conclude that the work optimum temperature of sample B is 200°C, while for sample A is 300°C. It means that (002)-oriented ZnO film has a better optimum working temperature because its optimum working temperature is lower than randomly oriented ZnO film.

Furthermore, gas sensor measurements with different NO gas concentrations (10-90 ppm) at 200°C were also performed. The dynamic response characteristic of ZnO films with five different concentration (10, 30, 50, 70, and 90 ppm) were shown in Fig.10 (a) which show an increasing response of ZnO films with the increase of NO gas concentration. It is well known that the ZnO films response is related to the NO gas adsorption on ZnO surface, where the number of NO gas molecule adsorbed on ZnO surface increase along with the increasing of NO gas concentration. That phenomenon results in increasing the response value. Based on a sensitivity curve in Fig.10 (b), it is obvious that ZnO nanorods film with (002) orientation has a higher gradient value compared to nanorods film with random orientation which indicates

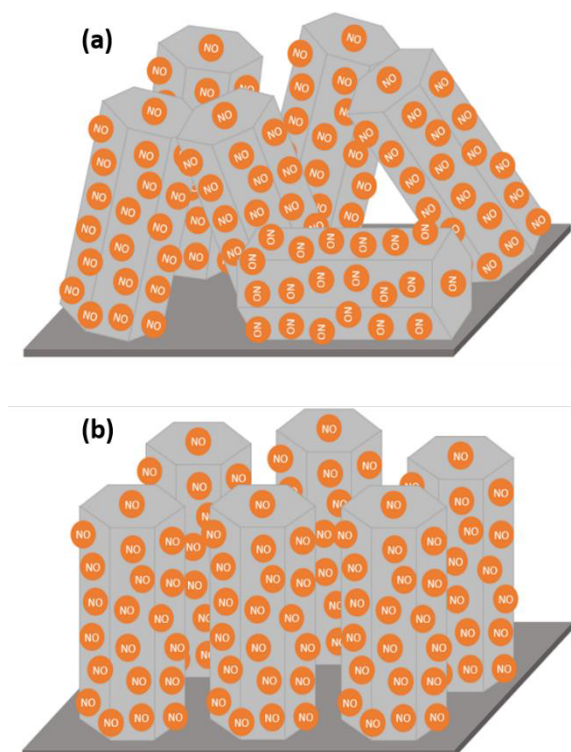


FIGURE 11. Illustration of active site of ZnO nanorods with (a) random orientation (b) (002) orientation.

that the ZnO nanorods film with (002) orientation has better sensitivity 0.19, than random orientation one 0.12. In the previous study, we also found that ZnO with (002) orientation gave the better result for CO detection than ZnO with random orientation [46]. However, the ZnO still displayed the best performance as a NO sensor.

From Fig.10 we also found that the ZnO nanorods film with (002) orientation shows a higher response than ZnO nanorods film with random orientation. It is well known that the surface ZnO act as an active site for target gas adsorption. ZnO nanorods film with random orientation has less active site than ZnO nanorods film with random orientation due to overlapping nanorods in random orientation will prevent the adsorption of target gas as illustrated in Fig.11. Consequently, ZnO nanorods film with random orientation has lower response than, ZnO nanorods film with (002) orientation. The higher performance of (002)-oriented ZnO is also caused by their higher density compare to random ZnO. According to our previous study, the denser the film or layer, the more active sites are available for sensing activity [5].

The result of the response and recovery time of ZnO films towards 30 ppm NO gas with different temperatures and at a fixed temperature of 200°C with different NO gas concentration are tested are shown in Table 1 and Table 2, respectively. According to the these results we know that the ZnO with (002) orientation has a faster response time and

TABLE 1. The response time and recovery time of ZNO films at various temperature.

Temperature	(002)-oriented ZnO film		Random-oriented ZnO film	
	Response time (s)	Recovery time (s)	Response time (s)	Recovery time (s)
160°C	420	210	420	350
200°C	290	160	405	95
250°C	275	100	395	85
300°C	240	85	250	70
350°C	220	40	125	10

TABLE 2. The response time and recovery time of ZNO films at various no gas concentration.

NO gas concentration	(002)-oriented ZnO film		Random-oriented ZnO film	
	Response time (s)	Recovery time (s)	Response time (s)	Recovery time (s)
10 ppm	430	100	465	90
30 ppm	295	130	410	100
50 ppm	285	145	355	140
70 ppm	270	150	325	150
90 ppm	220	180	205	170

a slower recovery time than ZnO films with random orientation. Therefore, ZnO film with (002) orientation performs better for NO gas sensing application than that of ZnO film with random orientation.

C. GAS SENSING MECHANISM AND SELECTIVITY

In this work, both A and B samples resistance decreased as the operational temperature increase indicate that they exhibited n-type semiconductor. Furthermore, at certain temperature, those n-type sample's resistance also decreased fastly when exposed to reducing gas like NO. Sequently, their resistance increased and reached baseline quickly after the flow stopped and the change of resistance is delivered as a sensor signal. The fast development of sensitive materials as gas sensor leaves the unclear mechanism, however, the involving of oxygen ionsorption is believed to contribute in the mechanism. Due to the energy activation of this reaction, oxygen ionsorption start to occur on the surface at 75°C [47], [48]. Above that temperature, oxygen from atmosphere will be adsorbed, dissociated, and ionized by taking electron from the conduction band of ZnO creating wide electron depletion layer lead to increase the resistance. The type of oxygen ion species resulted from this ionization depends on the operational temperature. O_2^- , O^- , and O^{2-} became predominance at 75-150°C, 150-200°C, and >200°C respectively according to Equation 2. At certain temperature, NO will adsorbed onto the surface of the oxide and react with the oxygen species, according to Equation 2, produce NO_2 as a product by releasing electron to the conduction band lead to decrease the resistance. As the gas sensor measurement testing showed 200°C is the optimum temperature, the surface reaction occurred

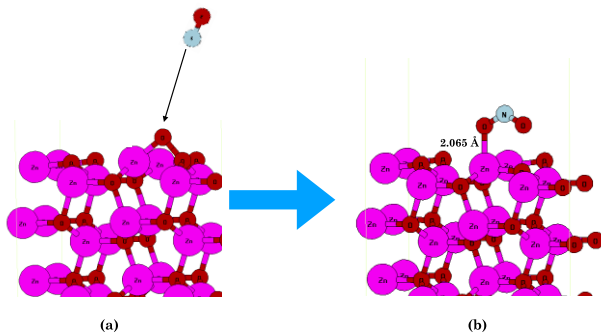
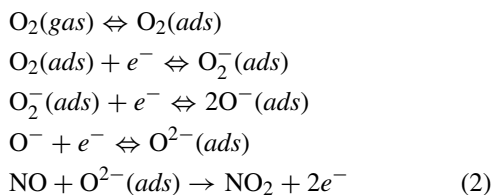


FIGURE 12. Initial configuration (a) and optimized geometry (b) of NO direct interaction with the O^{ads} site on the ZnO(100) surface.

mostly between NO and O^- species.



We performed atomic simulations using density functional theory-based calculations to support the mechanism of NO_2 formation from the reaction between NO gas and O ion on the ZnO surface in Equation 2. We used (100) surface facet to model the ZnO surface since this facet is the dominant surface facet for the nanorod morphology which is grown in the (002) direction. We added an oxygen adatom (O^{ads}) on the ZnO (100) surface to model the surface ionic oxygen (see Fig. 3). The most stable O^{ads} location for (100) surface is located on the top of the Zn-O dimer while for (002) surface the O^{ad} site is located on the hollow site. The conformation of O^{ads} site on the (100) surface is in agreement with previous DFT studies [49], [50].

The sensing process in Equation 2 involved the reaction between NO molecule and O adatom on the ZnO surface. Our calculation results suggest that this reaction can happen by two possible mechanisms. The first mechanism involves direct interaction between NO molecule and O^{ads} site. The incoming NO molecule directly attacks the O^{ads} site without undergoing adsorption process on the surface. This interaction results in a spontaneous formation of an adsorbed NO_2 molecule on the (100) surfaces as shown in Fig. 12. In the second mechanism, the incoming NO molecule is firstly adsorbed on one of the Zn atom site near O^{ads} site of ZnO(100) surface and then it interacts with the O^{ads} site to form NO_2 molecule (see Fig. 13). The NO_2 formations through this mechanism on the (100) surface is an activated process that requires activation energy of about 0.21 eV. This demonstrates that the formation of NO_2 through the second mechanism is also facile since it only requires small amount of activation energy. The results from these calculations prove the reaction mechanism which is suggested in Equation 2. The NO_2 molecule can be formed easily on the ZnO (100)

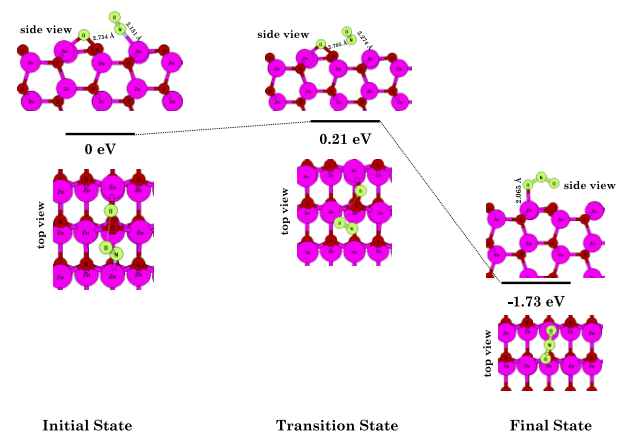


FIGURE 13. The initial state, transition state and final state of reaction between the adsorbed NO molecule and O^{ad} site on the ZnO(100) surface.

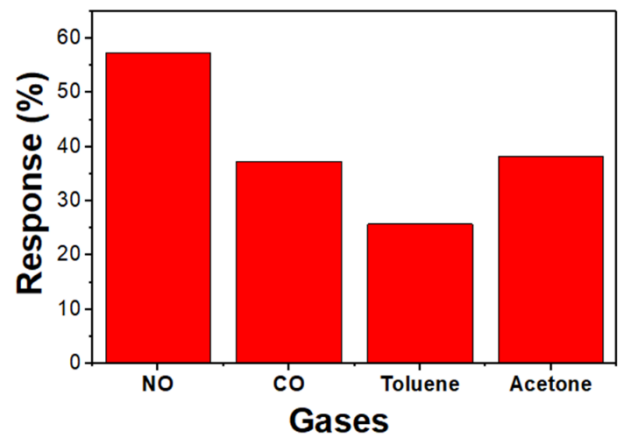


FIGURE 14. Selectivity of ZnO film with (002) orientation.

surface when NO molecule is directly exposed to the surface which has pre-adsorbed oxygen species.

Besides the gas response, the selectivity is another important property for ZnO film as a gas sensor. Fig.14 shows the response of (002)-oriented and randomly oriented ZnO film to NO, CO, toluene and acetone gas at 200°C. The concentration all gases were same, which is 30 ppm. From this figure we know that both ZnO films have a higher response when being exposed by NO gas than the other gases. This indicates that both ZnO films were more selective to detect the NO.

IV. CONCLUSION

In this paper, (002) oriented and randomly oriented ZnO film were successfully synthesized by Chemical Bath Deposition method. The orientation of ZnO films were controlled via the presence of DEA in seed layer precursor, where (002)-oriented and random-oriented ZnO film are synthesized by using DEA and without DEA, respectively. Furthermore, the gas sensing measurement shows that ZnO film with (002) orientation has a better performance for NO gas detection because it has a lower work optimum

temperature, a higher response and sensitivity, and a better selectivity than ZnO film with random orientation. These results indicate that (002)-oriented ZnO film is more potential for NO sensing application than that of randomly oriented ZnO film.

REFERENCES

- [1] *Right to Know Hazardous Substance Fact Sheets*, New Jersey Dept. Health, Trenton, NJ, USA, 2009.
- [2] H. J. Seo, R. H. Jeong, J. H. Boo, J. Song, and J. H. Boo, "Study on chemical removal of nitric oxide (NO) as a main cause of fine dust (air pollution) and acid rain," *Appl. Sci. Conver. Technol.*, vol. 26, pp. 218–222, Nov. 2017.
- [3] M. Wang, E. J. Kim, S. H. Hahn, C. Park, and K.-K. Koo, "Controlled crystal growth and crystallite orientation in ZnO films/nanorods prepared by chemical bath deposition: Effect of solvent," *Cryst. Growth Des.*, vol. 8, pp. 501–506, Jan. 2018.
- [4] Q. Li, J. Bian, J. Sun, J. Wang, Y. Luo, K. Sun, and D. Yu, "Controllable growth of well-aligned ZnO nanorod arrays by low-temperature wet chemical bath deposition method," *App. Surf. Sci.*, vol. 256, pp. 1698–1702, Jan. 2010.
- [5] B. Yulianto, M. F. Ramadhani, Nugraha, N. L. W. Septiani, and K. A. Hamam, "Enhancement of SO₂ gas sensing performance using ZnO nanorod thin films: The role of deposition time," *J. Mater. Sci.*, vol. 52, no. 8, pp. 4543–4554, Apr. 2017.
- [6] J. Xu, Y. Yu, X. He, J. Sun, F. Liu, and G. Lu, "Synthesis of hierarchical ZnO orientation-ordered film by chemical bath deposition and its gas sensing properties," *Mater. Lett.*, vol. 81, pp. 145–147, Aug. 2012.
- [7] H. Park, H. Ahn, S. H. Kim, and D. J. Kim, "ZnO nanorods on ZnO thin films with different preferred orientation and their Ethanol gas sensing properties," *J. Cer. Process. Res.*, vol. 17, pp. 632–636, Jun. 2016.
- [8] S. Roso, F. F. Güell, P. R. Martínez-Alanis, A. Urakawa, and E. Llobet, "Synthesis of ZnO nanowires and impacts of their orientation and defects on their gas sensing properties," *Sens. Actuators B, Chem.*, vol. 230, pp. 109–114, Jul. 2016.
- [9] H. T. Ng, J. Han, T. Yamada, P. Nguyen, Y. P. Chen, and M. Meyyappan, "Single crystal nanowire vertical surround-gate field-effect transistor," *Nano Lett.*, vol. 4, no. 7, pp. 1247–1252, May 2004.
- [10] M. Sinha, R. Mahapatra, B. Mondal, T. Maruyama, and R. Ghosh, "Ultrafast and reversible gas-sensing properties of ZnO nanowire arrays grown by hydrothermal technique," *J. Phys. Chem. C*, vol. 120, no. 5, pp. 3019–3025, 2016.
- [11] S. B. Jagadale, V. L. Patil, S. A. Vanalakar, P. S. Patil, and H. P. Deshmukh, "Preparation, characterization of 1D ZnO nanorods and their gas sensing properties," *Ceramics Int.*, vol. 44, pp. 3333–3340, Feb. 2017.
- [12] T. Mitsuyu, S. Ono, and K. Wase, "Structures and SAW properties of RF-sputtered single-crystal films of ZnO on sapphire," *J. Apply. Phys.*, vol. 51, pp. 2464–2470, Jul. 1980.
- [13] M. T. Man, J.-H. Kim, M. S. Jeong, A. T. Do, and H. S. Lee, "Oriented ZnO nanostructures and their application in photocatalysis," *J. Lumin.*, vol. 185, pp. 17–22, May 2017.
- [14] M.-C. Kao, H.-Z. Chen, S.-L. Young, C.-C. Lin, and C.-Y. Kung, "Structure and photovoltaic properties of ZnO nanowire for dye-sensitized solar cells," *Nano. Res. Lett.*, vol. 7, p. 260, Dec. 2012.
- [15] G. S. Kino and R. S. Wagers, "Theory of interdigital couplers on nonpiezoelectric substrates," *J. Appl. Phys.*, vol. 44, pp. 1480–1488, Apr. 1973.
- [16] Y. S. Ho and K. Y. Lee, "Fabrication of highly oriented (002) ZnO film on glass by sol-gel method," *Thin Solid Films*, vol. 519, pp. 1431–1434, Dec. 2010.
- [17] D. Guo, K. Sato, S. Hibino, T. Takeuchi, H. Bessho, and K. Kato, "Low-temperature preparation of (002)-oriented ZnO thin films by sol-gel method," *Thin Solid Films*, vol. 550, pp. 250–258, Jan. 2014.
- [18] S. Kahraman, F. Bayansal, H. A. Cetinkara, H. M. Cakmak, and H. S. Guder, "Characterization of CBD grown ZnO films with high c-axis orientation," *Mater. Chem. Phys.*, vol. 134, pp. 1036–1041, Jun. 2012.
- [19] T.-H. Lee, H. Ryu, and W.-J. Lee, "Fast vertical growth of ZnO nanorods using a modified chemical bath deposition," *J. Alloys Compounds*, vol. 597, pp. 85–90, Jun. 2014.
- [20] X. Zhang, S. Ma, F. Li, F. Yang, J. Liu, and Q. Zhao, "Effects of substrate temperature on the growth orientation and optical properties of ZnO: Fe films synthesized via magnetron sputtering," *J. Alloys Compounds*, vol. 574, pp. 149–154, Oct. 2013.
- [21] C. H. Chao, P. W. Chi, and D. H. Wei, "Investigations on the crystallographic orientation induced surface morphology evolution of ZnO thin films and their wettability and conductivity," *J. Phys. Chem. C*, vol. 120, pp. 8210–8219, Mar. 2016.
- [22] H. S. Kang, J. S. Kang, J. W. Kim, and S. Y. Lee, "Annealing effect on the property of ultraviolet and green emissions of ZnO thin films," *J. Appl. Phys.*, vol. 95, pp. 1246–1250, Jan. 2004.
- [23] P. B. Taunk, R. Das, D. P. Bisen, R. K. Tamrakar, and N. Rathor, "Synthesis and optical properties of chemical bath deposited ZnO thin film," *Karbala Int. J. Modern Sci.*, vol. 1, no. 3, pp. 159–165, Nov. 2015.
- [24] N. Saadaldin, M. N. Alsloom, and N. Hussain, "Preparing of copper oxides thin films by chemical bath deposition (CBD) for using in environmental application," *Energy Procedia.*, vol. 74, pp. 1459–1465, Aug. 2015.
- [25] L. Znaidi, "Sol-gel-deposited ZnO thin films: A review," *Mater. Sci. Engineer. B*, vol. 174, pp. 18–30, Oct. 2010.
- [26] N. H. Ha, D. D. Thinh, N. T. Huong, N. H. Phuong, P. D. Thach, and H. S. Hong, "Fast response of carbon monoxide gas sensors using a highly porous network of ZnO nanoparticles decorated on 3D reduced graphene oxide," *App. Surf. Sci.*, vol. 434, pp. 1048–1054, Mar. 2018.
- [27] J. P. Perdew, K. Burke, and M. Ernzerhof, "Generalized gradient approximation made simple," *Phys. Rev. Lett.*, vol. 77, pp. 3865–3868, Oct. 1996.
- [28] J. Y. Jung, "Involvement of Bcl-2 family and caspases cascade in sodium fluoride-induced apoptosis of human gingival fibroblasts," *Korean J. Physiol. Pharmacol.*, vol. 10, pp. 289–295, Oct. 2006.
- [29] P. Giannozzi, "QUANTUM ESPRESSO: A modular and open-source software project for quantum simulations of materials," *J. Phys. Condens. Matter.*, vol. 21, no. 39, Jan. 2009, Art. no. 395502.
- [30] P. E. Blöchl, "Projector augmented-wave method," *Phys. Rev. B, Condens. Matter*, vol. 50, pp. 17953–17979, Dec. 1994.
- [31] P. Erhart, K. Albe, and A. Klein, "First-principles study of intrinsic point defects in ZnO: Role of band structure, volume relaxation, and finite-size effects," *Phys. Rev. B, Condens. Matter*, vol. 73, May 2006, Art. no. 205203.
- [32] Q.-L. Tang and Q.-H. Luo, "Adsorption of CO₂ at ZnO: A surface structure effect from DFT+U calculations," *J. Phys. Chem. C*, vol. 117, pp. 22954–22966, Oct. 2013.
- [33] S. Grimme, "Semiempirical GGA-type density functional constructed with a long-range dispersion correction," *J. Comput. Chem.*, vol. 27, no. 15, pp. 1787–1799, Nov. 2006.
- [34] A. Kokalj, "Computer graphics and graphical user interfaces as tools in simulations of matter at the atomic scale," *Comput. Mater. Sci.*, vol. 28, pp. 155–168, Oct. 2003.
- [35] G. Henkelman, G. Johansson, and H. Jónsson, "Methods for finding saddle points and minimum energy paths," in *Theoretical Methods in Condensed Phase Chemistry*. Dordrecht, The Netherlands: Springer, 2002, pp. 269–300.
- [36] G. Henkelman, G. Jóhannesson, and H. Jónsson, "Improved tangent estimate in the nudged elastic band method for finding minimum energy paths and saddle points," *J. Chem. Phys.*, vol. 113, pp. 9978–9985, Nov. 2000.
- [37] G. Henkelman, B. P. Uberuaga, H. Jónsson, and G. A. Henkelman, "A climbing image nudged elastic band method for finding saddle points and minimum energy paths," *J. Chem. Phys.*, vol. 113, pp. 9901–9904, Nov. 2000.
- [38] F. Boudjouan, A. Cjelouche, T. Touam, D. Djouadi, S. Khodja, M. Tazerout, Y. Ouerdane, and Z. Hadjoub, "Effects of stabilizer ratio on photoluminescence properties of sol-gel ZnO nano-structured thin films," *J. Lumin.*, vol. 158, pp. 32–37, Feb. 2015.
- [39] W. Zeng, M. Wu, Y. Li, and S. S. Wu, "Hydrothermal synthesis of different SnO₂ nanosheets with CO gas sensing properties," *J. Mater. Sci., Mater. Electron.*, vol. 24, no. 10, pp. 3701–3706, Oct. 2013.
- [40] Q. Jia, H. Ji, Y. Zhang, Y. Chen, X. Sun, and Z. Jin, "Rapid and selective detection of acetone using hierarchical ZnO gas sensor for hazardous odor markers application," *J. Hazardous Mater.*, vol. 276, pp. 262–270, Jul. 2014.
- [41] A. A. Firooz and A. Akbari, "Highly sensitive CO sensors based on star-like ZnO nanostructures," *J. Mater. Sci., Mater. Electron.*, vol. 27, no. 11, pp. 11488–11494, Nov. 2016.
- [42] S. Bhatia, N. Verma, and R. K. Bedi, "Ethanol gas sensor based upon ZnO nanoparticles prepared by different techniques," *Result Phys.*, vol. 7, pp. 801–806, Feb. 2017.
- [43] A. Singh, A. Sharma, M. Tomar, and V. Gupta, "Growth of highly porous ZnO nanostructures for carbon monoxide gas sensing," *Surf. Coat. Tech.*, vol. 343, pp. 49–56, Jun. 2018.

- [44] L. Zhua, W. Zenga, H. Yeb, and Y. Li, "Volatile organic compound sensing based on coral rock-like ZnO," *Mater. Res. Bull.*, vol. 100, pp. 259–264, Apr. 2018.
- [45] C. Wang, L. Yin, L. Zhang, D. Xiang, and R. Gao, "Metal oxide gas sensors: Sensitivity and influencing factors," *Sensors*, vol. 10, no. 3, pp. 2088–2106, Jan. 2010.
- [46] F. Fitriana, N. L. W. Septiani, I. Irzaman, F. Ferdiansjah, M. Z. Fahmi, D. R. Adhika, S. Suyatman, N. Nugraha, and B. Yulianto, "Preparation of (002)-oriented ZnO for CO gas sensor," *Mater. Res. Express*, vol. 6, Mar. 2019, Art. no. 064003.
- [47] S. Lenaerts, J. Roggen, and G. Maes, "FT-IR characterization of tin dioxide gas sensor materials under working conditions," *Spectrochimica Acta A, Mol. Spectrosc.*, vol. 51, no. 5, pp. 883–894, May 1995.
- [48] S. C. Chang, "Oxygen chemisorption on tin oxide: Correlation between electrical conductivity and EPR measurements," *J. Vac. Sci. Technol.*, vol. 17, p. 366, Jun. 1988.
- [49] Y. Yan, M. M. Al-Jassim, and S. H. Wei, "Oxygen-vacancy mediated adsorption and reactions of molecular oxygen on the ZnO(10 $\bar{1}$ 0) surface," *Phys. Rev. B, Condens. Matter*, vol. 72, Oct. 2005, Art. no. 161307.
- [50] H. Xu, R. Q. Zhang, and S. Y. Tong, "Interaction of O₂, H₂O, N₂, and O₃ with stoichiometric and reduced ZnO(10 $\bar{1}$ 0) surface," *Phys. Rev. B, Condens. Matter*, vol. 82, Oct. 2010, Art. no. 155326.



DAMAR RASTRI ADHIKA received the bachelor's degree in engineering physics from the Institut Teknologi Bandung (ITB), the master's degree in biomedical engineering from the University of Applied Sciences Lübeck, and the Ph.D. degree from the Kyushu University on Materials Engineering, especially on the study of material deformation and fracture mechanics at nanoscale level. She has been a Faculty at the Engineering Physics Study Program, Institut Teknologi Bandung (ITB), Indonesia, since 2016. She is currently a Staff with the Research Center for Nanosciences and Nanotechnology, ITB. For the past 3 years, she has been working with electron microscopes for material characterization and has several projects on composite material and image processing.



ADHITYA GANDARYUS SAPUTRO received the B.S. degree from the Engineering Physics Department, Institut Teknologi Bandung, Indonesia, and the Ph.D. degree from the Applied Physics Department, Osaka University, Japan. He is currently a Faculty Member with the Department of Engineering Physics, Faculty of Industrial Technology, Institut Teknologi Bandung. His current research interest includes surface and interface science.



FITRIANA received the B.Sc. degree in physics from the University of Jember, Jember, in 2014, and the M.Sc. degree in physics engineering from the Institut Teknologi Bandung, in 2018. His current research interest includes surrounds nanomaterials, especially ZnO, for chemiresistive-type gas sensor.



NUGRAHA received the B.S. degree from the Engineering Physics Department, Institut Teknologi Bandung, Bandung, Indonesia, and the master's and Ph.D. degrees from Tohoku University, Tohoku, Japan. He is currently an Associate Professor with the Department of Engineering Physics, Faculty of Industrial Technology, Institut Teknologi Bandung, Bandung, Indonesia. His current research interests include crystal growth and nanomaterials for energy and environment application.



NI LUH WULAN SEPTIANI received the B.Sc. degree in physics from the Indonesia University of Education, Bandung, Indonesia, and the M.Sc. degree in engineering physics from the Institut Teknologi Bandung, Bandung, Indonesia, where she is currently pursuing the Ph.D. degree. Her current research interest includes the development of nanocomposite material for environmental application.



BRIAN YULIARTO received the B.S. degree from the Engineering Physics Department, Institut Teknologi Bandung, Bandung, Indonesia, and the M.Eng. and Ph.D. degrees from the Department of Quantum Engineering and Systems Science, The University of Tokyo, Tokyo, Japan. He is currently a Full Professor with the Department of Engineering Physics, Faculty of Industrial Technology, Institut Teknologi Bandung, where he is also the Head. His current research interests include nanomaterials development for energy and environmental application. He have published more than 50 articles in his research area.

...